Engineering Fracture Mechanics 189 (2018) 1–12

Contents lists available at ScienceDirect

Engineering Fracture Mechanics

journal homepage: www.elsevier.com/locate/engfracmech

Comparative assessment of the fracture behaviour of micro-alloyed and API-5L X65 steels in simulated fuel grade ethanol environment

O.O. Joseph [a,b,*], C.A. Loto [a,c], S. Sivaprasad [b], J.A. Ajayi [d], S. Tarafder [b]

[a] Department of Mechanical Engineering, Covenant University, P.M.B. 1023, Canaanland, Ota, Nigeria
[b] CSIR-National Metallurgical Laboratory, Jamshedpur 831007, India
[c] Department of Chemical, Metallurgical and Materials Engineering, Tshwane University of Technology, P.M.B. X680, Pretoria, South Africa
[d] Department of Metallurgical and Materials Engineering, Federal University of Technology, P.M.B. 704, Akure, Nigeria

ARTICLE INFO

Article history:
Received 16 September 2016
Received in revised form 4 August 2017
Accepted 6 August 2017
Available online 14 October 2017

Keywords:
Steels
Fracture mechanics
Ductile fracture
Fuel ethanol

ABSTRACT

In order to fully realize the benefit of pipeline and automotive materials in fuel ethanol applications, a comprehensive understanding of their fracture behaviour is essential. Very few studies have been undertaken on fracture of materials in stress corrosion environments. This paper presents a comparative assessment of the fracture toughness, tearing modulus and widths of stretch zones for API-5L X65 steel and micro-alloyed steel (MAS). The results show that MAS exhibits a better fracture resistance than API-5L X65 steel in air and in solution. API-5L X65 in solution shows a faster crack extension than MAS-in solution. It is found that J_{str} (fracture toughness derived from stretch zone geometry) obtained for the two steels exhibits a similar trend with J_i (initiation fracture toughness) which is obtained at the departure of the blunting line on their *J-R* curves and thus suitable for representing the initiation toughness of the two steels in solution. In general, fuel ethanol reduces fracture resistance in X65 and micro-alloyed steels.

1. Introduction

Due to the stress corrosion cracking failures often encountered in fuel ethanol end-user storage and blending facilities, fracture mechanics based analysis is crucial in order to predict the behaviour of applicable materials. Infrastructure plays a key role in ensuring safe, reliable and efficient distribution of fuels to end-users. Materials which normally are compatible with gasoline may be damaged by the presence of ethanol in the fuel. Consequently, a substantial number of notched slow-strain rate (N-SSR) tests have been conducted to study stress corrosion cracking initiation and propagation mechanisms of steels in fuel ethanol [1,2–8,9]. API-5L X52 carbon steel was reported to exhibit ductile fracture in the presence of 0.5–2 vol% water content in simulated E95 blend [9]. Crack growth rate increased with increasing ethanol concentration in N-SSR tests performed with X46 double submerged arc weld (DSAW) line pipe steel [10]. Crack growth rates of a seamless line pipe, cast steel and a low frequency electric resistance weld (LFERW) pipe are to a certain extent lower than for a DSAW pipe [10].

Additionally, the influences of simulated fuel-grade ethanol (SFGE) on fatigue crack propagation have been thoroughly evaluated for several pipeline and storage-tank steels. A36, X52 and X70 pipeline steels are susceptible to enhanced fatigue

* Corresponding author at: Department of Mechanical Engineering, Covenant University, P.M.B. 1023, Canaanland, Ota, Nigeria.
E-mail address: funmi.joseph@covenantuniversity.edu.ng (O.O. Joseph).

https://doi.org/10.1016/j.engfracmech.2017.08.012
0013-7944/

Nomenclature

σ_o, σ_{YS}, σ_{UTS}	flow stress, yield stress, ultimate tensile stress
%	percent
v	Poisson's ratio
ΔK	stress intensity factor range
a_i, a_{oq}, Δa_Q	instantaneous crack length, original crack length, crack extension
b_o, $b_{(i-1)}$	un-cracked ligament, at the start of test and at (i − 1)th step
e_u, e_T	uniform elongation, total elongation
n	strain hardening exponent as per Hollomon's equation
$A_{pl(i)}$	instantaneous area under the load-plastic load line displacement curve in fracture toughness test
B, B_N	specimen thickness, net specimen thickness
E	elastic modulus
H_v	Vickers hardness
$J_{0.2}$, J_i, J_{IC}, J_{pl}, J_{str}	an energy based fracture parameter, determined at 0.2 mm crack extension, initiation fracture toughness, qualified as plane strain fracture toughness, plastic part of fracture toughness, fracture toughness measured from stretch zone
K_i	instantaneous stress intensity factor
P_i	instantaneous load
S	specimen span
W	specimen width
T_R	tearing slope at critical crack extension

damage attributable to ethanol stress-corrosion cracking in fuel-grade ethanol environments [11]. It is worth noting that in spite of the investigations carried out so far, there are still growing concerns about the SCC behaviour of pipelines used to handle fuel ethanol. Similarly, not many studies using fracture mechanics techniques for steels in alcoholic stress corrosion environments have been made [12–17]. In addition, there is dearth of information on fracture toughness of steels in recently emerged fuel ethanol environments.

It is with a view to extending knowledge in this area of study that this research seeks to center its investigation on the fracture study of API-5L X65 and micro-alloyed steels in E20 simulated fuel ethanol environment with respect to a reference fracture behaviour in air. The effect of environment on fracture toughness, tearing resistance and stretch zone widths (SZW) of the two steels were investigated.

2. Experimental procedures

2.1. Materials

The API-5L X65 and micro-alloyed steels (MAS) used in this investigation were commercially produced rolled pipes and plates respectively. They have application in the automotive and pipeline industries. The X65 pipe was ~560 mm outer diameter with ~7 mm wall thickness. The micro-alloyed steel plate was 7 mm in thickness. The chemical composition of the as-received steels is shown in Table 1.

Specimens were fabricated for tensile and monotonic *J*-integral tests from the stock materials under as-received condition. Fabrication of tensile test specimens was in accordance with ASTM E8M-15a [18]. Round tensile specimens of 5 mm gauge diameter were fabricated from MAS whereas rectangular specimens were used for the API-5L X65 tensile test. Table 2 lists the mechanical properties of the two steels which were obtained from tensile tests at room temperature. The tensile flow curve of the steels exhibited prominent yield point effects. The microstructures of the two steels are shown in Fig. 1. Both steels consisted of predominantly ferritic structure with pearlite randomly oriented in the ferrite matrix. The MAS material contains larger-grained polygonal ferrite relative to the API-5L X65 material and thus accounts for its lower yield strength (301 MPa).

To evaluate fracture behaviour, three-point bend (TPB) specimens as shown in Fig. 2 were employed for carrying out monotonic *J-R* tests in air and fuel-ethanol solution (E20). The orientation of the specimens were LT (in case of MAS) and

Table 1
Chemical composition of MAS and API-5L X65 steels in as-received condition (wt.%).

Element	C	Mn	Si	Cr	Ni	Al	Ti	Mo	Cu	Fe
MAS	0.13	0.77	0.012	0.027	0.015	0.042	0.0025	0.0017	0.006	Balance
API-5L X65	0.08	1.22	0.245	0.022	0.023	0.026	0.0029	0.0062	0.008	Balance

Table 2
Mechanical properties of MAS and API-5L X65 steels in as-received condition.

Sample	σ_{YS} (MPa)	σ_{UTS} (MPa)	e_u (%)	e_T (%)	n#	Log k	H_v^*
MAS	301	458	18	38	0.13	2.5	111
API-5L X65	482	570	14	39	0.07	2.7	175

Tensile properties reported are average of two tests, with ±2% variation. H_v^* denotes average hardness from seven readings; n# from $\sigma = k\varepsilon^n$.

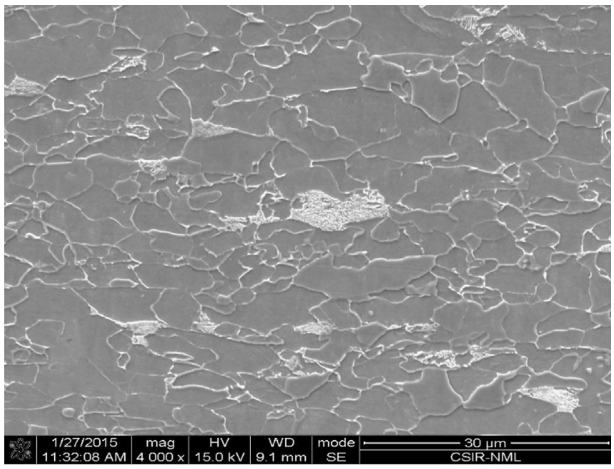

(a)

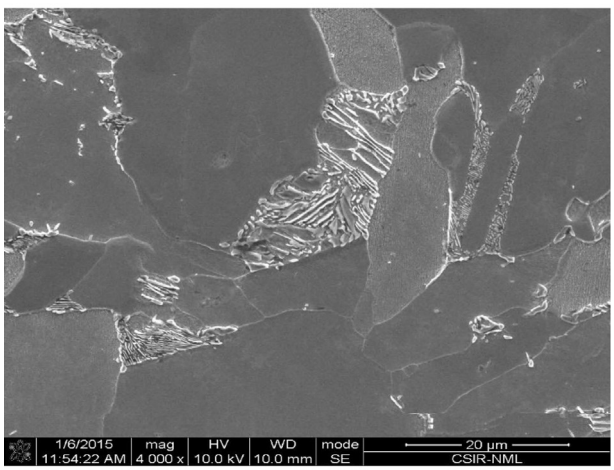

(b)

Fig. 1. Microstructure of (a) API-5L X65 steel and (b) MAS in as-received condition showing the presence of ferrite and pearlite phases.

LC (in case of API 5LX65 pipe). The nominal width of TPB specimens used was 20 mm. The nominal thickness was 7 mm. The span (distance between the rollers) employed to conduct the test was four times the width of the specimen. It may be noted that specimen thickness chosen was close to the full thickness of the stock material. Specimens were fabricated by wire-cut electro-discharge machining (EDM) in order to ensure high levels of precision and alignments demanded for fracture mechanics specimens. All specimens were provided with integral knife edges for compliance based crack length measurement. Specimens were fatigue precracked under constant ΔK of 15 MPa$\sqrt{}$m, R-ratio of 0.1, K_{max} of 16.7 MPa$\sqrt{}$m and a frequency of 5 Hz in servohydraulic testing systems interfaced to computers for test control and data acquisition. Samples were set to precrack up to $a/W = 0.5$ (where a and W are crack length and width of the specimen respectively) using a 5 mm COD gage with a travel of 2 mm.

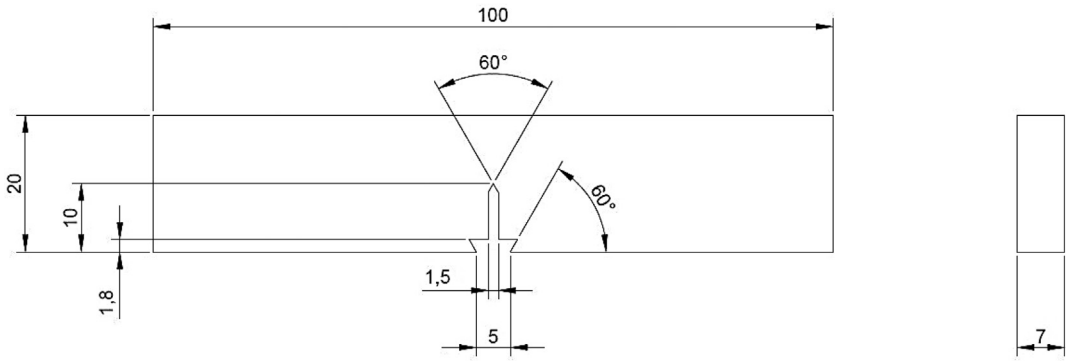

Fig. 2. Schematic of specimen configuration and dimension for three-point bend test (mm).

2.2. Test environment

The test solution was prepared partly in accordance with ASTM D-4806-07 [19] for fuel grade ethanol. Simulated fuel-ethanol (E20) environment was prepared using 195 proof ethanol absolute. Other reagents added include: pure methanol, glacial acetic acid, ultra-pure water (~18 MΩ·cm) and pure sodium chloride (NaCl) with purity >99%. NaCl was first dissolved in water, and then added to ethanol to reach the specified NaCl and water concentrations respectively. The baseline composition for the simulated fuel-grade ethanol used in this study is shown in Table 3. All reagents used were of analytical grade. E20 fuel-ethanol blend was prepared by adding 4 L unleaded gasoline to 1 L SFGE. The ethanol-based fracture test was carried out and interpreted with respect to a reference test conducted in air.

2.3. Fracture toughness testing

Single specimen unloading compliance method was employed for carrying out fracture toughness tests as per the procedures laid down in ASTM Standard E1820 [20]. This standard contains the method for determining elastic-plastic fracture mechanics (EPFM) ductile fracture parameter J_{Ic}. The ramp rate was 10^{-04} mm/s for loading, 10^{-02} mm/s for unloading and 10^{-02} mm/s for reloading. Loading was carried out very slowly at the ramp rate of 10^{-04} mm/s in each sequence in order to enhance SCC effect if any. A relatively fast unloading was employed so as to avoid unnecessary time over-run to complete the tests and the tensile stress required for promoting SCC (if any) was not removed for a longer duration. Crack lengths were calculated by monitoring the specimen compliance at each unloading. A 10 mm gauge length COD gauge with 4 mm travel fitted across the knife edges of the specimen is used for this purpose. Tests were sustained until well beyond the maximum load bearing capacity of the specimens to ensure substantial crack extension, and comprised of approximately 60 intermediate unloadings. A commercial software was used for test control and data acquisition. Considering the time consumed for the test, a single test was conducted under each condition. All tests were carried out at room temperature (27 °C). A special containment used for the test is shown in Fig. 3. The container was attached to the base of the test frame and the bend fixture was connected to the actuator piston. Approximately, 5 L of fresh solution was used in each test, such that the fatigue pre-cracked portion of the specimen was completely immersed, leaving the integral knife-edge for safe attachment of the COD gauge.

The crack length a at each instance of unloading was calculated from the elastic compliance C of the unloading curve using compliance crack length relations as described elsewhere [21]. The energy parameter J for the instant of ith unloading was calculated incrementally using

$$J_{(i)} = \frac{(K_{(i)})^2(1-\nu^2)}{E} + J_{pl(i)} \tag{1}$$

$$\text{where} \quad K_{(i)} = \left[\frac{P_i S}{(B \cdot B_N)^{1/2} W^{3/2}}\right] f(a_i/W) \quad \textit{and} \tag{2}$$

Table 3
Composition of simulated fuel ethanol (partly) based on ASTM D 4806 [19].

Ethanol (vol%)	Methanol (vol%)	Water (vol%)	NaCl (mg/L)	Acetic acid (mg/L)
98.5	0.5	1	32	56

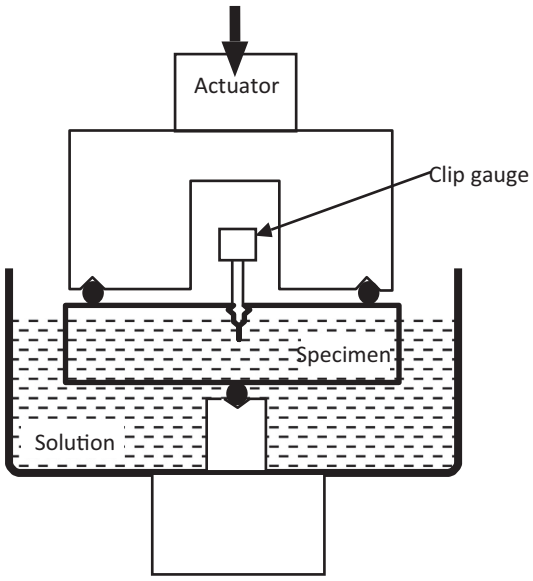

Fig. 3. Three-point bend test set-up for the ethanol solution-based test.

$$f(a_i/W) = \frac{3(a_i/W)^{1/2}\left[1.99 - \left(\frac{a_i}{W}\right)\left(1-\frac{a_i}{W}\right)\left(2.15 - 3.93\left(\frac{a_i}{W}\right) + 2.7\left(\frac{a_i}{W}\right)^2\right)\right]}{2\left(1+2\frac{a_i}{W}\right)\left(1-\frac{a_i}{W}\right)^{3/2}} \tag{3}$$

$$J_{pl(i)} = \left[J_{pl(i-1)} + \left(\frac{\eta_{pl}}{b_{(i-1)}}\right)\left(\frac{A_{pl(i)} - A_{pl(i-1)}}{B_N}\right)\right]\left[1 - \gamma_{pl}\frac{a_{(i)} - a_{(i-1)}}{b_{(i-1)}}\right] \tag{4}$$

$K_{(i)}$ is the stress intensity factor calculated from the instantaneous load P_i and the crack length a_i, v is the Poisson's ratio, η and γ are geometry and crack dependent factors, $A_{pl(i)}$ is the area under the load-plastic part of the LLD curve, B_N is the net specimen thickness and $b_{(i-1)}$is the incremental remaining crack ligament.

The load, load line displacement (LLD) and crack mouth opening displacement (CMOD) data were processed post-test to obtain *J-R* curves. The iterative procedures suggested in ASTM standard E-1820 [20] for obtaining the experimental blunting line slope m, the power law fit of the form $J = C_1(\Delta a)^{C_2}$ (where C_1 and C_2 are constants) to data points within the tearing part of the resistance curve, and the adjusted initial crack length a_{oq}, are employed in the *J-R* analysis. As a result of the high toughness of the steels being investigated and insufficient stock material thickness, the ASTM criteria for qualifying J_{Ic} were found not to be satisfied and a plane strain fracture toughness parameter could not be obtained. For the given thickness, therefore, the intersection of the blunting line with the power law curve is considered as the initiation toughness J_i and that of with the 0.2 mm offset blunting line was considered as $J_{0.2}$.

2.4. Fractography

Fracture surfaces produced through the *J* integral tests were observed under a scanning electron microscope. Specific attention was paid to record the stretch zone that forms ahead of the fatigue precrack before the tearing extension of the crack through microvoid coalescence.

3. Results and discussion

3.1. Tensile and fracture behaviour

The tensile deformation behaviour of the two steels is shown in Fig. 4. As may be inferred from the figure, API-5L X65 steel exhibited an appreciable yield point elongation following a sharp yield point in comparison to micro-alloyed steel. In the case of micro-alloyed steel, an elastic-plastic transition was clearly visible but a sharp yield drop was not significant. The difference in the tensile behaviour of both steels can be attributed to the difference in the microstructures of the two steels [22]. A larger grain sized ferritic structure as in the case of micro-alloyed steel is liable to have lower yield strength. API-5L X65 exhibits yield strength that is 60% higher than that of MAS. The tensile properties of the two steels are presented in Table 2. On the whole, API-5L X65 steel shows higher strength properties and concurrently marginally low ductility (consid-

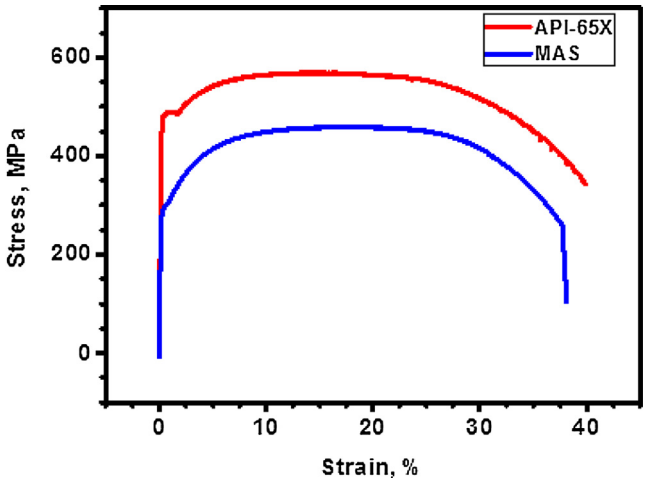

Fig. 4. Stress-strain curves of API-5L X65 and MAS tensile tests.

ering the uniform elongation) in comparison to micro-alloyed steel. This is significant from the perspective that fracture toughness is liable to be lower for materials with higher strengths and low ductility [21].

Typical load–displacement records obtained from the *J-R* test are shown in Fig. 5. Concurrent with the dissimilarity between the tensile properties of MAS and API-5L X65 steel, their fracture characteristics were found to be different in E20 fuel ethanol environment. From Fig. 5, it can be seen that the two materials exhibited significant ductile tearing. Furthermore, a comparison of the load versus load-line displacement plots for the materials shows substantial deformation prior to reaching load maxima for the cases with MAS. This is indicative of high toughness associated with low strength and high ductility of MAS.

On the other hand, the reference tests conducted in air revealed close similarity in the *J-R* curves of both steels as shown in Fig. 6. From the layout of the *J-R* curves, it can be seen that API-5L X65 steel and MAS displays identical resistance to stable crack extension in air. Studies have shown that a comparison based on the shape and layout of the *J-R* curves can frequently be misleading, hence it is appropriate to base assessments on the critical fracture toughness parameter [23].

Accordingly, the initiation toughness, J_i and the (unqualified) critical fracture toughness at 0.2 mm ductile crack extension $J_{0.2}$ were determined. The value of $J_{0.2}$ was estimated to be 630 kJ m^{-2} for MAS and 536 kJ m^{-2} for API-5L X65 steel. Considering the higher strength of API-5L X65 steel, this is logically acceptable. In addition, it was found that for the two steels, the slope of the blunting line of the *J-R* curve is higher than the empirical value of $2\sigma_o$ (σ_o representing the flow stress); a slope of $\sim 6\sigma_o$ and $\sim 5\sigma_o$ was calculated from the experimental data for MAS and API-5L X65 steel respectively.

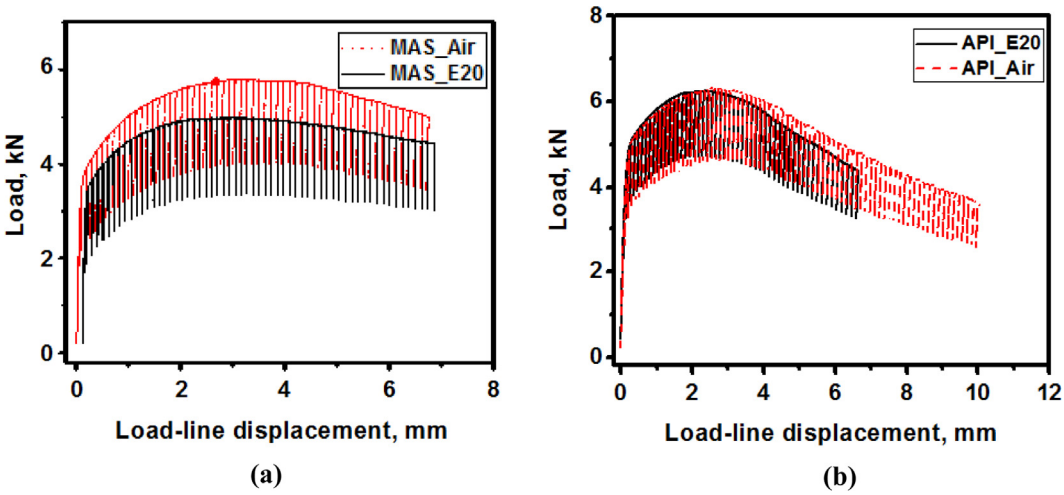

Fig. 5. Typical load-displacement plots of (a) MAS and (b) API-5L X65 in fuel-ethanol (E20) environments.

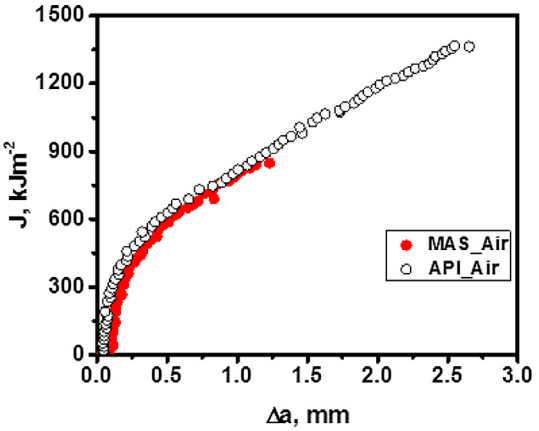

Fig. 6. *J-R* curves for MAS and API-5L X65 in air.

3.2. Effect of fuel-ethanol (E20) on fracture toughness

With the introduction of fuel ethanol environment, the *J-R* behaviour of MAS and API-5L X65 steel was altered. The fracture resistance of MAS decreases (Fig. 7), in the presence of fuel ethanol environment, as compared to air. Similarly, for API-5L X65 steel, fuel ethanol environment essentially decreased its resistance to stable crack extension with respect to air as shown in Fig. 8. It is therefore apparent that the ethanolic solution resulted in decreasing fracture resistance for both materials. Furthermore, it may be pointed out that a steeper J-R curve denotes an enhanced resistance of the material to fracture [21]. It was also observed that the alteration of the test environment changed the blunting line for MAS significantly whereas for API-5L X65, the change was insignificant. In addition, the critical fracture toughness was noticeably altered due to the presence of fuel ethanol environment. In Fig. 9, the identification of $J_{0.2}$ on a *J-R* curve, as per the methods of ASTM standard E-1820 for a particular case of API-5L X65 specimen is shown.

The variation of fracture toughness $J_{0.2}$ with the test environment for the two steels is presented in Table 4. There is decrease in fracture toughness in ethanol environment. Though an apparent decrease in $J_{0.2}$ is noted, the actual percentage reduction is only 8–9% with respect to air data. The initiation toughness is therefore not significantly affected by the environment in both steels. From Table 2 and Fig. 3, it may be noted that the strain hardening exponent is significantly higher in MAS as compared to API-5L X65. The strain hardening capacity of the material indicates the spread of plastic strain that essentially controls the crack tip blunting process. A higher strain hardening is thus expected to result in substantial crack tip blunting and higher initiation toughness, as compared to a material with lower strain hardening index. This shows that the initiation process is largely controlled by the strain hardening behaviour of the material.

However, the fracture toughness obtained for MAS in air and in E20 fuel ethanol environment is significantly higher than that of API-5L X65 in similar test conditions. Thus, it appears that the MAS material has a superior resistance to fracture than API-5L X65 steel.

Table 4 shows the values of $J_{0.2}$, tearing modulus (T_R) and the specimen thickness criteria required for qualifying $J_{0.2}$ to J_{IC}. Table 4 shows that none of the values of $J_{0.2}$ obtained for both the steels are not qualified to be termed as J_{IC} as per ASTM 1820 [20] criteria. This means that the fracture toughness values are size dependent and therefore amenable to comparisons only with specimens of similar size [24].

3.3. Effect of fuel-ethanol (E20) on tearing modulus

While fracture initiation toughness provides some information about the fracture behaviour of a ductile material, the entire *J-R* curve gives a more complete description. The slope of the *J-R* curve at a given amount of a crack extension is indicative of the relative stability of the crack growth. The tearing modulus or propagation resistance, T_R can be used to examine the stable ductile tearing regime of the *J–R* curve and can be experimentally determined following equation (5) [25].

$$T_R = (dJ/da)(E/\sigma_o) \tag{5}$$

where dJ/da is the tearing slope of the *J–R* curve beyond crack initiation point, E is the elastic modulus of the material and σ_o is the flow stress of the material.

Using Eq. (5), T_R was determined for all test conditions and comparison of resistance to crack extension is made in Table 4 for both steels. For MAS, resistance to crack extension was found to increase with changing test environment. This indicates substantial crack tip dissolution with prolonged exposure to the environment. A blunted crack tip can significantly decrease the state of stress ahead of the crack tip thereby improving the ductile tearing process, represented by a high tearing resistance (T_R). In addition, the competition between active anodic dissolution and repassivation ahead of the crack tip controls

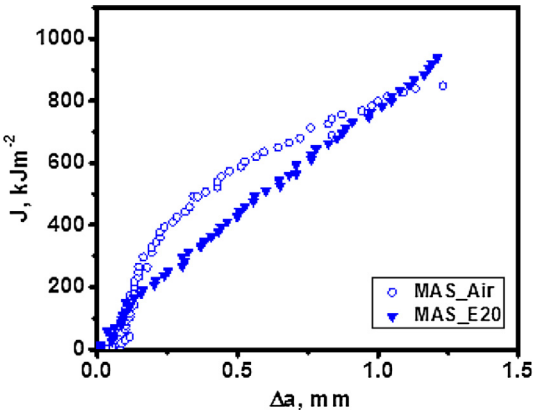

Fig. 7. *J-R* curves obtained from MAS specimens.

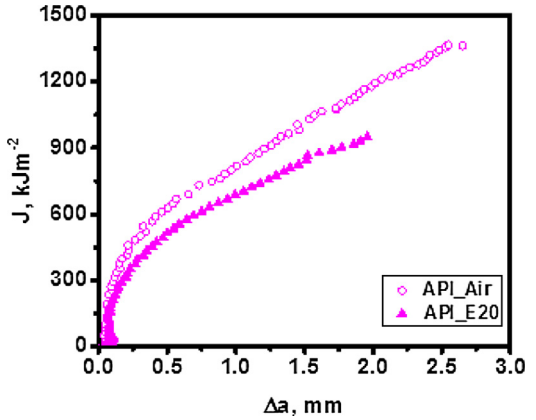

Fig. 8. *J-R* curves obtained from API-5L X65 specimens.

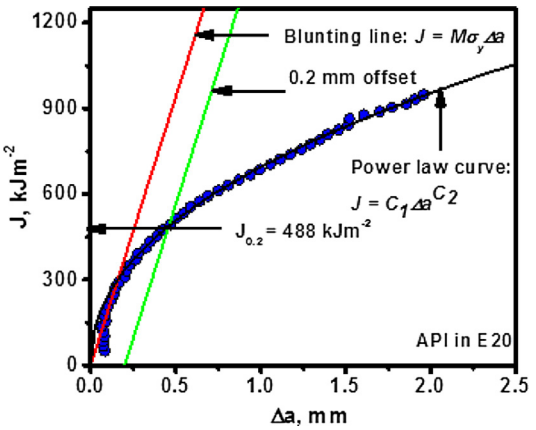

Fig. 9. Identification of $J_{0.2}$ on the *J-R* curve obtained from an API-5L X65 specimen.

Table 4
Qualifying criteria for fracture toughness $J_{0.2}$ for MAS and API-5L X65 steel.

Environmental Condition	Temperature (°C)	B (mm)	b_o (mm)	σ_o (MPa)	$J_{0.2}$ (kJ/m^2)	T_R
MAS_Air	27	6.96	9.54	379	630	0.46
MAS_fuel-ethanol (E20)	27	6.91	9.10	379	576	0.87
API_Air	27	6.98	9.68	525	536	0.51
API_ fuel-ethanol (E20)	27	6.97	9.66	525	488	0.45

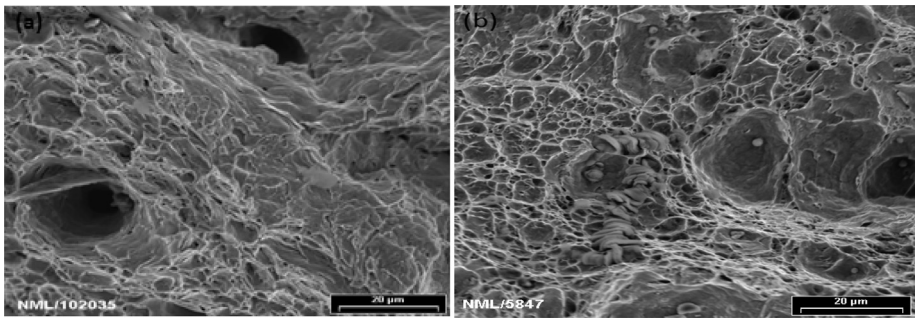

Fig. 10. Fracture surface of (a) MAS and (b) API-5L X65 steel after monotonic J test in air.

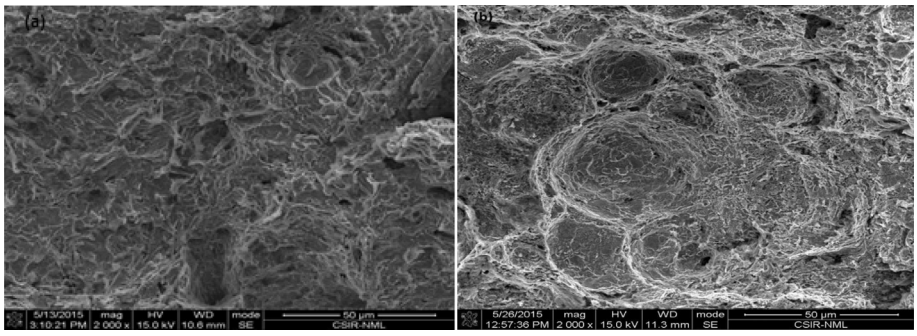

Fig. 11. Fracture surface of (a) MAS and (b) API-5L X65 steel after monotonic J test in fuel-ethanol (E20).

the propagation of these cracks [26]. The load versus load-line displacement plots, *J-R* curves and T_R of MAS confirms its slow tearing behaviour in fuel-ethanol. On the contrary, API-5L X65 steel showed a decrease in T_R. Apparently, the crack tip has not been sufficiently blunted due to corrosion damage (crack tip dissolution) in this steel and a decrease in stable crack growth resistance is also an indication of fracture mechanisms other than microvoid coalescence that control the crack extension process.

Fig. 10 shows the fracture mechanism of MAS and API-5L X65 steel after J testing in air. Both fracture surfaces depicts ductile tearing as the prevalent fracture mechanism when the materials were tested in air. Nevertheless, upon exposure to fuel-ethanol environment, MAS exhibited microvoid coalescence and inter-pearlitic cleavage, characteristic of mixed ductile and brittle behaviour due to increased tearing resistance (Fig. 11a) whereas in API steel (Fig. 11b), the voids were shallower and wider, indicating an insufficient strain accommodation by during void growth.

3.4. Effect of fuel-ethanol (E20) on widths of stretch zones

Crack extension by void coalescence is preceded by the expanse of stretch zone, which is a featureless region that forms immediately after the fatigue precrack region. The stretch zone essentially forms to accommodate the plastic strains that are required for void growth ahead of the crack. When the process of crack extension through coalescence of voids with the blunted crack tip is initiated, continual extension of the crack by similar process is certain owing to the availability of matured voids further ahead [21]. Customarily, in extremely ductile materials, stretch zone would have two components *viz*., stretch zone width (*SZW*) and stretch zone depth (*SZD*). Both *SZW* and *SZD* are closely related to fracture toughness. Nevertheless, there is no agreement regarding which of these stretch zone measurements should be used for defining critical

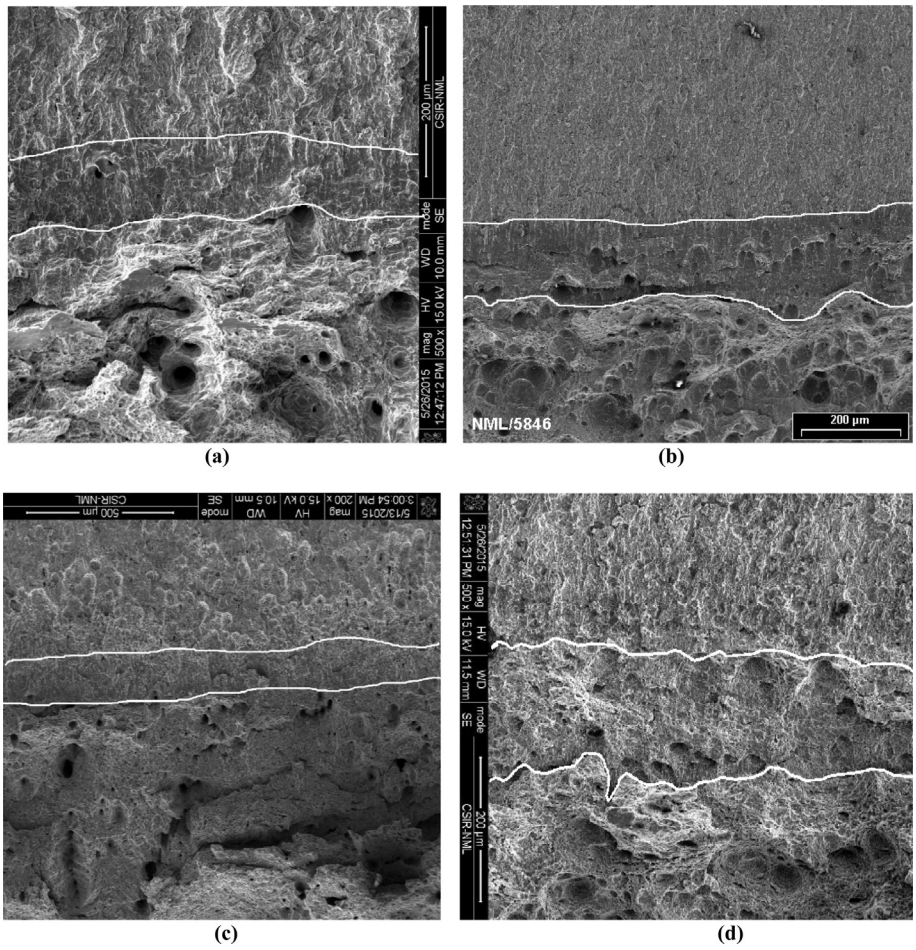

Fig. 12. Fractographs of MAS and API-5L X65 showing the stretch zone region with delineated boundaries. (a) MAS_Air, (b) API_Air, (c) MAS_E20 + 32 mg/L NaCl and (d) API_E20 + 32 mg/L NaCl.

Table 5
A comparison of J_i, J_{SZW} and J_{str} values for MAS and API-5L X65 steel.

Material	Air			Fuel-ethanol (E20)		
	J_i (kJ/m^2)	SZW (µm)	J_{str} (kJ/m^2)	J_i (kJ/m^2)	SZW (µm)	J_{str} (kJ/m^2)
MAS	265	103	190	193	144	156
API-5L X65	334	177	396	323	267	371

fracture toughness. Some researchers have used *SZW* [27–31] while others have used *SZD* [32,33] for obtaining ductile fracture toughness.

The values of J_i obtained in this investigation were compared with SZW dimensions, as the width of the stretch zone essentially corresponds to the critical crack extension (Δa_{cr}) prior to the onset of fracture process. Stretch zone features were recorded using SEM and typical stretch zone features are presented in Fig. 12. Measurements of SZW were carried out on a series of fractographs representing almost the entire stretch zone region across the specimen thickness. The boundaries of the stretch zones were delineated manually to enable measurement.

It may be noted that for MAS in all the environment test conditions, there was lack of clarity in defining the stretch zone as shown in Fig. 12a whereas, for API-5L X65 steel, the stretch zone was clearly identified in all the tested specimens as shown in Fig. 12b. The SZW is not uniform along the crack front; as a result, a number of measurements were used to arrive at average values. The fractographs were obtained at a magnification of 200x.

It has been reported [27] that J_{str} is identical to J_i, which is obtained at the departure of the *J-R* curve from the blunting line. In *J-R* curve, intersection of a projection on x-axis corresponding to Δa = SZW, should give the initiation toughness, called J_{str} which is equal to J_i determined at the departure of the *J-R* curve from its initial regime. Such an exercise was

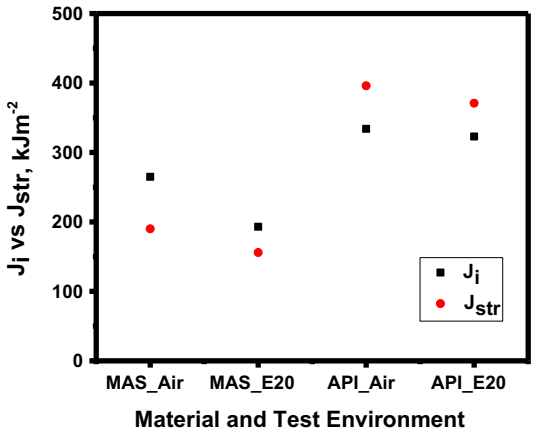

Fig. 13. Variation of J_i and J_{str} with test environment for MAS and API-5L X65 steel.

attempted for micro-alloyed and API-5L X65 steels and for MAS, the width of the stretch zone was used to obtain the J_{str} from the *J-R* curves as presented in Table 5. Fig. 13 shows that J_{str} values obtained for both MAS and API-5L X65 steel from their respective SZW values are close to the J_i obtained at the departure from the linear portion of their *J-R* curves. This indicates that the notion of crack tip blunting through stretching and subsequent initiation of crack extension that is used to model fracture behaviour is also applicable for materials tested in solution. Hence, it is proposed that stretch zone widths can be used to determine the initiation toughness of steels in solution. A comparative assessment of the behaviour of MAS and API-5L X65 steel in air and fuel-ethanol, with respect to their J_i, SZW and J_{str} values points out a decrease in crack tip blunting of MAS in the presence of fuel-ethanol. However, fuel-ethanol does not seem to show any significant effect on initiation toughness in X65 steel.

4. Conclusions

An overview of the fracture behaviour of API-5L X65 and micro-alloyed steels in fuel-ethanol has been presented in this paper. From the experimental results of the three-point bending tests, it was concluded that micro-alloyed steel possesses a superior resistance to fracture in comparison to API-5L X65 steel in fuel ethanol environment. The tearing resistance of API-5L X65 steel suffered drastic reductions upon imposition of monotonic unloading in fuel-ethanol whereas for MAS, an increase in tearing resistance was observed. Ductile crack extension through microvoid coalescence is suppressed in MAS due to the absence of adequate stress triaxiality at the crack tip that supports and promotes void generation and growth. The notion of crack tip blunting through stretching is applicable for fracture tests in solution. Hence, it is proposed that stretch zone widths can be used to determine the initiation toughness of steels in solution.

Acknowledgements

This work was sponsored by CSIR-National Metallurgical Laboratory, Jamshedpur, India and The World Academy of Sciences (TWAS), Trieste, Italy [grant number 3240275047].

References

[1] API. Technical report 939-D, stress corrosion cracking of carbon steel in fuel-grade ethanol: review, experience survey, field monitoring and laboratory testing. Washington DC: American Petroleum Institute; 2007.
[2] Anand V, Brian C, Russell DK, Ken K. Evaluation of stress corrosion cracking behavior of steel in multiple ethanol environments, https://www.onepetro.org/conference-paper/NACE-10077, ; 2010 [accessed 14 March 2010].
[3] Cao L. Corrosion and stress corrosion cracking of carbon steel in simulated fuel grade ethanol Dissertation. Ohio State University; 2012.
[4] Goodman L, Singh PM. Effects of chemical composition of ethanol fuel on carbon steel pipelines, www.sbpmat.org.br/icam2009dir/submission/autor/arquivos/BB723.pdf, ; 2009 [accessed 25 September 2009].
[5] Lou X, Yang D, Goodman RL, Singh PM. Understanding the stress corrosion cracking of X-65 pipeline steel in fuel grade ethanol, https://www.onepetro.org/conference-paper/NACE-10073, ; 2010 [accessed 18 March 2010].
[6] McIntyre DR, Kane RD, Venkatesh A. SCC behavior of steel in fuel ethanol and butanol, https://www.onepetro.org/conference-paper/NACE-09530, ; 2009 [accessed 26 March 2009].
[7] Venkatesh A, Chambers B, Kane RD, Kirkham K. Evaluation of stress corrosion cracking behavior of steel in multiple ethanol environments, https://www.onepetro.org/conference-paper/NACE-10077, ; 2010 [accessed 18 March 2010].
[8] Lou X, Yang D, Singh PM. Effect of ethanol chemistry on stress corrosion cracking of carbon steel in fuel-grade ethanol. Corrosion 2009;65:785–97.
[9] Pedraza-Basulto GK, Arizmendi-Morquecho AM, Cabral Miramontes JA, Borunda Terrazas A, Martinez-Villafone A, Chacon-Nava JG. Effect of water on the stress corrosion cracking behaviour of API 5L–X52 steel in E95 blend. Int J Electrochem Sci 2013;8:5421–37.
[10] Beavers J, Sridhar N, Zamarin C. Effects of microstructure and ethanol-gasoline blend ratio on SCC of ethanol pipelines, https://www.onepetro.org/conference-paper/NACE-09532, ; 2009 [accessed 26 March 2009].

[11] Sowards JW, Weeks TS, McColskey JD. The influence of simulated fuel-grade ethanol on fatigue crack propagation in pipeline and storage-tank steels. Corros Sci 2013;75:415–25. doi: https://doi.org/10.1016/j.corsci.2013.06.026.
[12] Hugh IL. Studies of the stress-corrosion cracking of low-carbon steels. J Res Nat Bur Stand-C 1962;66C:347–56.
[13] Johnson HH, Willner AM. Moisture and stable crack growth in high strength steel. Appl Mater Res 1965;4:34–40.
[14] Fessler RR, Barlo TJ. Threshold-stress determination using tapered specimens and cyclic stresses. ASTM STP 821 1984:368–82. doi: https://doi.org/10.1520/STP34443S.
[15] Hauser JA, Crooker TW. An investigation of stress-corrosion cracking susceptibility in candidate steels for tension leg platform tendons, http://oai.dtic.mil/oai/oai?verb=getRecord&metadataPrefix=html&identifier=ADA167286, ; 1986 [accessed 24 April 1986].
[16] Dong Y. Factors affecting stress assisted corrosion cracking of carbon steel under industrial boiler conditions Dissertation. Georgia Institute of Technology; 2008.
[17] Dayal RK, Parvathavarthini N. Hydrogen embrittlement in power plant steels. Sadhana 2003;28:431–51.
[18] ASTM E8/E8M-15a. Standard test method for tension testing of metallic materials. West Conshohocken (PA, USA): ASTM International; 2015.
[19] ASTM-D-4806-07. Standard specification for denatured fuel ethanol for blending with gasoline for use as automotive spark-ignition engine fuel. West Conshohocken (PA, USA): ASTM International; 2007.
[20] ASTM E1820-08a. Standard test method for measurement of fracture toughness. West Conshohocken (PA, USA): ASTM International; 2008.
[21] Tarafder S, Sivaprasad S, Ranganath VR. Comparative assessment of fatigue and fracture behaviour of cast and forged railway wheels. Fatigue Fract Eng Mater Struct 2007;30:863–76.
[22] Sivaprasad S, Tarafder S, Ranganath VR, Ray KK. Effect of prestrain on fracture toughness of HSLA steels. Mater Sci Eng A 2000;284:195–201.
[23] Das SK, Sivaprasad S, Das S, Chatterjee S, Tarafder S. The effect of variation of microstructure on fracture mechanics parameters of HSLA-100 steel. Mater Sci Eng A-Struct 2006;431:68–79.
[24] Joseph OO, Loto CA, Sivaprasad S, Ajayi JA, Tarafder S. Role of chloride in the corrosion and fracture behaviour of micro-alloyed steel in E80 simulated fuel grade ethanol environment. Materials 2016;9:463. doi: https://doi.org/10.3390/ma9060463.
[25] Anderson TL. Fracture mechanics, fundamentals and applications. USA: CRC Press Inc.; 2004.
[26] Baena LM, Gomez M, Calderon JA. Aggressiveness of a 20% bioethanol-80% gasoline mixture on autoparts: I behaviour of metallic materials and evaluation of their electrochemical properties. Fuel 2012;95:320–8.
[27] Sivaprasad S, Tarafder S, Ranganath VR, Das SK, Ray KK. Can stretch zone measurements provide a good estimate of fracture toughness?, http://wwwicfweb.org/documents/proceedings/icf10-honolulu-hawaii-2001, ; 2001 [accessed 6 December 2001].
[28] Ranganath VR, Kumar AN, Pandey RK. Fracture toughness characterization of a weldment in a microalloyed steel using resistance curves. Mater Sci Eng 1991;132:153–60.
[29] Bassim MN, Mathews JR, Hyatt CV. Evaluation of fracture toughness of HSLA 80 steel at high loading rates using stretch zone measurements. Eng Fract Mech 1992;43:297–303.
[30] Pandey RK, Sundaram S, Kumar AN. Critical assessment of methods for J_{IC} evaluation. J Test Eval 1992;20:106–13.
[31] Amouzouvi KF, Bassim MN. Determination of fracture toughness from stretch zone width measurement in predeformed AISI type 4340 steel. Mater Sci Eng 1982;55:257–62.
[32] Cao WD, Lu XP. On the relationship between the geometry of deformed crack tip and crack parameters. Int J Fract 1984;25:33–52. doi: https://doi.org/10.1007/BF01152748.
[33] Sreenivasan PR, Ray SK, Vaidyanathan S, Rodriguez P. Measurement of stretch zone height and its relationship to crack tip opening displacement and initiation J-value in an AISI 316 stainless steel. Fatigue Fract Eng Mater Struct 1996;19:855–68. doi: https://doi.org/10.1111/j.1460-2695.1996.tb01021.x.